Study of the 3-(3,3-Dimethylbutanoyl)-4-hydroxy-6-neopentyl-2H-pyran-2-one by IR, Raman spectroscopy, and DFT

V.L. Furer[a*], A.E. Vandyukov[c], E.I. Nomerotskaya[b], M.M. Mukhtarova[b], V.V. Kovalev[b], V.I. Kovalenko[c]

[a]*Kazan State Architect and Civil Engineering University, 1 Zelenaya, 420043 Kazan, Russia*

[b]*Department of Chemistry, Moscow State University, 1-3 Lenin's Hills, 119991 Moscow, Russia*

[c]*A.E. Arbuzov Institute of Organic and Physical Chemistry, RAS, 8 Arbuzov Str., 420088 Kazan, Russia*

Abstract

The heterocyclic structure of pyrones has a variety of biological activities and plays an important role in the creation of new drugs. Therefore, the study of the structure and spectra of pyrones is of considerable interest. In this work, we studied the IR and Raman spectra of 3-(3,3-Dimethylbutanoyl)-4-hydroxy-6-neopentyl-2H-pyran-2-one (**1**) in its crystalline state. The tautomerization of **1** was followed by a quantum-chemical method at the DFT/B3LYP/6-311G** level. The calculation for the 4-hydroxy enol tautomer (A) reproduces the experimental IR and Raman spectra of compound **1**. The classification of the bands in the experimental vibrational spectra of **1** has been carried out. The intramolecular H-bond was characterized by IR spectroscopy.

The free energies of the tautomers and their populations were calculated for two different solvents. It appears from our data that tipe *A* dominates. The content of tautomer *B* increases in the nonpolar solvent but does not exceed 13%. As can be seen from our calculations and experimental X-ray data, the pyran ring of the molecule is flat.

HOMO and LUMO of molecule **1** are located on the pyran ring. During tautomeric transformations, there is a significant delocalization of charge and a change in the reactivity of the molecule. The reactivity of pyrone **1** was characterized using descriptors. The form *B* was found to have higher ionization energy, electron affinity, chemical potential, and electrophilic index than the *A* form. The dipole moment is higher for form *A*, and the softness of the two molecules is the same.

Keywords: Acids, IR spectra, Raman spectra, Hydrogen bonds, Normal vibrations, DFT

* Tel.: +7-843-5104737; fax.: +7-843-2387972. E-mail address: furer@kgasu.ru (V.L. Furer).

1. Introduction

The study of heterocyclic pyrone derivatives is interesting and important because they are used in the pharmaceutical, cosmetic, and food industries [1–5]. Pyrones are biologically active substances and are used for the manufacture of analgesics, anti-cancer drugs, and to fight against HIV [1−10]. Pyrones are the initial reagents in the synthesis of many organic compounds [1−10]. Studies on NMR spectra have shown that among the five tautomeric forms of the pyrones, two enolic forms predominate [11, 12]. The IR and NMR spectra of pyrones have been studied [13−18].

Our work for the first time characterized the two low-energy tautomeric forms of the 3-(3,3-dimethylbutanoyl)-4-hydroxy-6-neopentyl-2H-pyran-2-one (**1**) using the methods of IR and Raman spectroscopy and quantum chemistry. The choice of compound **1** is linked to the tautomerism of the central structural fragment of pyrandione, which can modify certain features characteristic of the functional groups. The enamine derivative of synthesized pyrone **1** has inhibitory activity against the human carcinoma cell line HeLa and the herpes virus VPG [19]. We attempted to trace the change in the structure of the acid, the strength of the hydrogen bond and its vibrational spectra during tautomeric transformations. The comparison of the free energies of the tautomers makes it possible to estimate their population.

It was important to follow the evolution of the geometry, electronic structure, and spectra of pyrone **1** during tautomeric transformations. Active centers of the molecule for nucleophilic and electrophilic attacks have been determined. The calculation of the charges on the acid atoms made it possible to estimate the capacity of the atoms to form hydrogen bonds and attract ions and metal atoms. The electrophilicity index characterizes the biological activity of compound **1**.

2. Material and method

2.1. Experimental

The neopentyl derivative of dehydroacetic acid 3-(3,3-dimethylbutanoyl)-4-hydroxy-6-neopentyl-2H-pyran-2-one (**1**) has been obtained by $CF_3SO_3H/(CF_3CO)_2O$ activated acylation of carboxylic acids according to [19, 20]. The white product has the crystalline powder form (melting point 77−78°C). Compound **1** can exist in two tautomeric enol forms, *A* and *B* (Fig. 1).

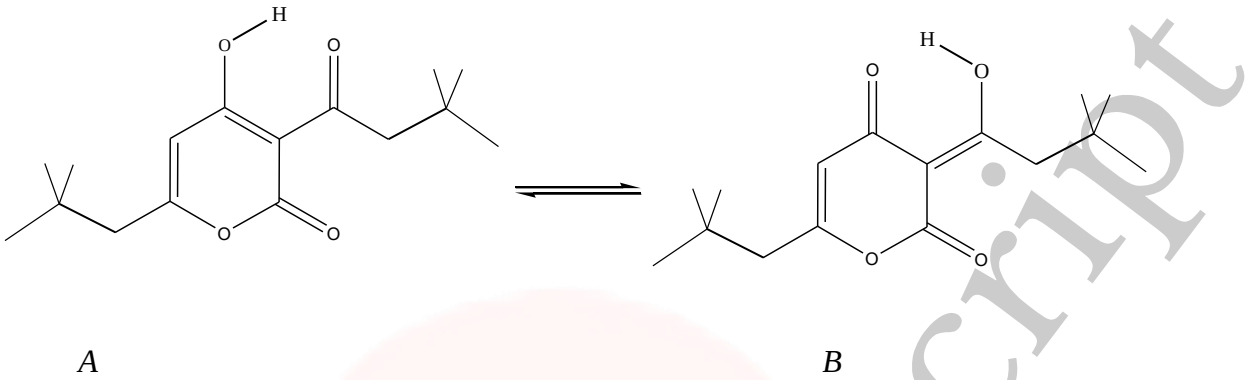

A *B*

Fig. 1. The structure of tautomeric forms *A* and *B* of compound **1**.

IR spectra were recorded by accumulating 64 scans in the region of 4000–400 cm^{-1} with a resolution of 4 cm^{-1}. A Bruker Vector 22 spectrometer was used [21]. The samples were compressed into KBr pellets.

Raman spectra of the pyrone were recorded in the 3500-50 cm^{-1} region via the FTIR spectrometer VERTEX 70 and the Bruker FT-Raman RAM II module [21]. The 1064 nm excitation line provided by an Nd:YAG laser with a power of 50 mW was used.

2.2. Computational details

The calculation of the vibrational spectra of compound **1** was carried out with the functional B3LYP [22, 23] and the basis set 6-311G**. The calculations were performed using the Gaussian09 program [24]. As a first approximation, we took the experimental coordinates of the atoms obtained using the X-ray diffraction method (Supplementary Information S1). Standard optimization methods were used to find minima on the potential surface. Full geometry optimization was performed without any restrictions. The Hessian analysis made it possible to determine the minima of potential energy.

Optimized geometrical parameters of the tautomers were used to calculate the harmonic vibration frequencies. Theoretical structural and spectral data were obtained for both tautomers at 298 K, 1 atm. The potential energy distribution was calculated to attribute the vibrations [25]. Calculated frequencies were scaled using a multiplier of 0.96. The theoretical spectral curves were constructed, taking the Lorentz band shape and a half-width of 10 cm^{-1}.

The calculation of natural bonding orbitals (NBO) has been performed to characterize the electronic properties of molecules [26]. The chemical potential, hardness, softness, and electrophilicity index are related to the first vertical ionization energy and electron affinity by the following formulas: $\mu \approx -(IE + EA)/2$, $\eta \approx (IE - EA)$,

$S=1/\eta$, and $\omega=\mu^2/2\eta$ [27]. The Fukui functions for nucleophilic $f_k^+(r)=[q_k(N+1)-q_k(N)]$ and electrophilic $f_k^-(r)=[q_k(N)-q_k(N-1)]$ attacks were calculated using the natural atomic charges on atoms q_k and the number of electrons N in a molecule. The local softness of atoms has also been calculated $s_k^+ = Sf_k^+, s_k^- = Sf_k^-$ [27].

Using the difference in free energies of the tautomers, their populations at 298.15 K can be calculated $p = \frac{\exp(-\Delta G_i/RT)}{\sum_j \exp(-\Delta G_j/RT)}$ [28]. A polarizable continuum model was used to assess the influence of the polar environment on the tautomeric equilibrium [28].

3. Results and discussion

3.1. Structural analysis

As can be seen from the X-ray diffraction data in the crystalline state at room temperature, the *A* tautomer of compound **1** is realized (Supplementary Information S1). In the more stable tautomer *A*, an intramolecular hydrogen bond is realized. The measured distance between the O3 and O4 atoms is 2.437 Å. Supplementary Information S2 lists the measured bond lengths and angles of tautomer *A*.

The results of geometry optimization of tautomers *A* and *B* are shown in Fig. 2 and in Supplementary Information S2. Gibbs's free energy and Boltzmann weights of tautomers are shown in Table 1. It appears from our data that type *A* dominates. The content of tautomer *B* increases in the less polar chloroform but does not exceed 13%. Vibrational spectra were calculated for tautomers *A* and *B*.

As can be seen from our calculations and experimental X-ray data, the pyran ring of the molecule is flat. A satisfactory agreement is observed between the calculated geometrical parameters of tautomer *A* and the experimental X-ray data.

Bond lengths change during tautomeric transformation. In tautomeric form *A*, the calculated bond lengths are (Å) 1.313 (O(3)–C(7)), 1.250 (O(4)–C(27)), 1.413 (C(6)–C(7)), and 1.467 (C(6)–C(27)), and for the *B* tautomer, the length of these bonds changes to 1.259, 1.302, 1.458, and 1.411, respectively. Such changes in bond lengths are consistent with the change in their properties during the tautomeric transformation. The H-bond lengths in the *A* and *B* tautomers are also different. The calculated O(3)···O(4) distances for tautomers *A* and *B* are 2.473 and 2.418 Å, respectively.

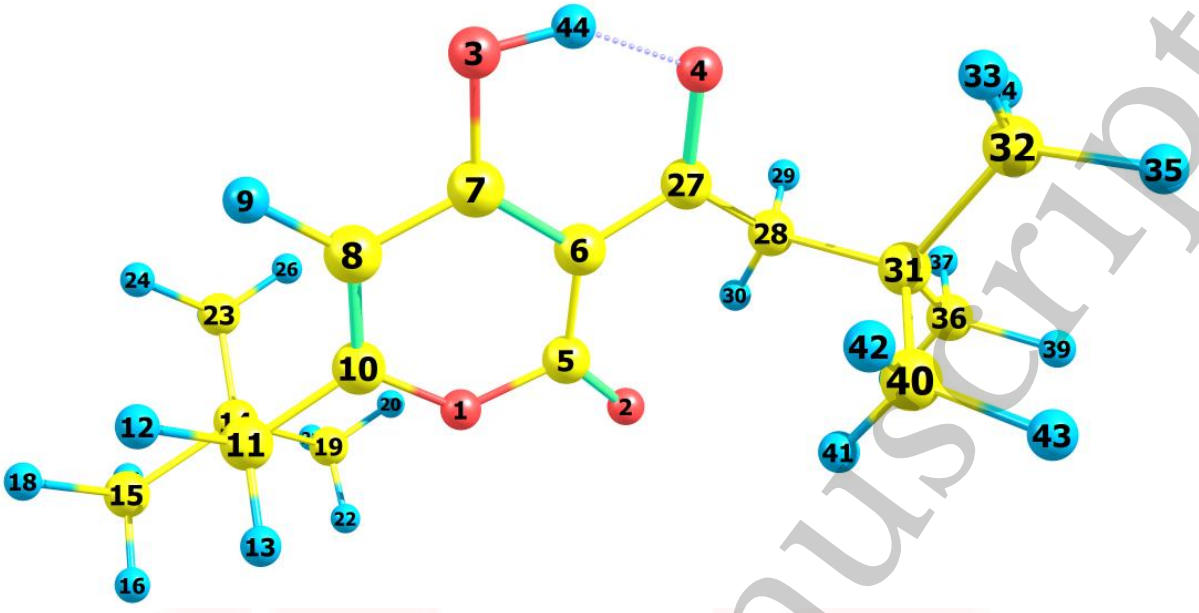

(1)

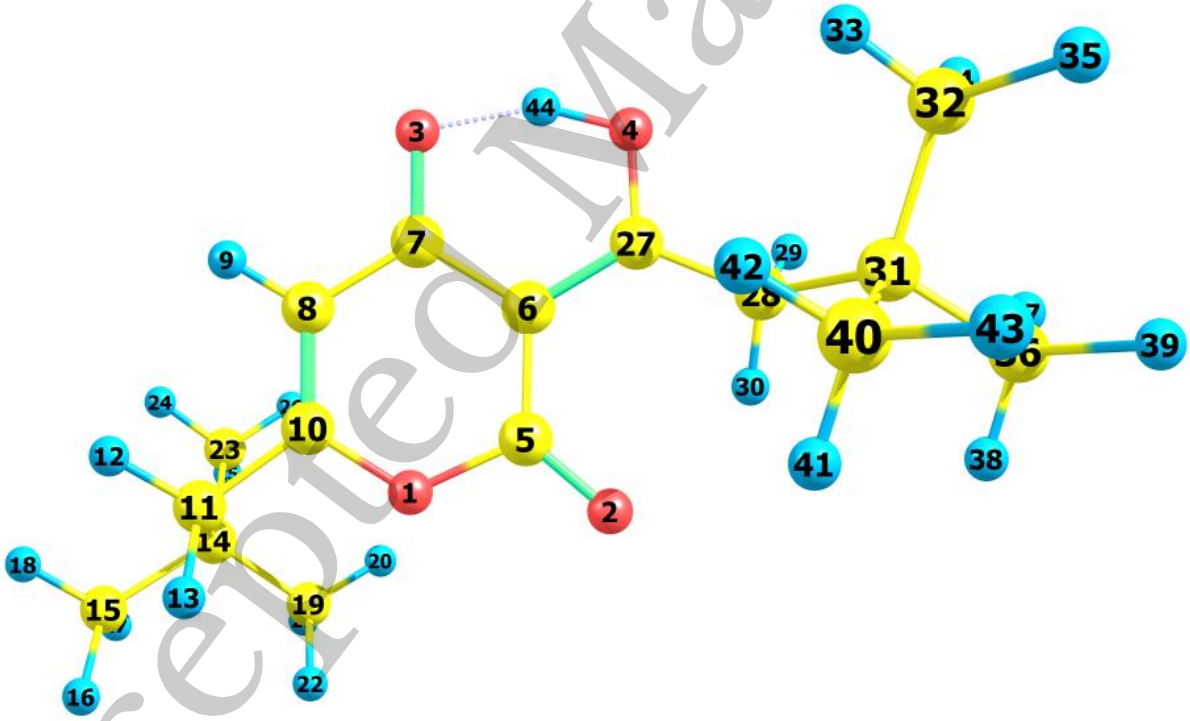

(2)

Fig. 2. Geometry and atom numbering for tautomeric forms *A* (1) and *B* (2) of compound **1**.

Table 1

Gibbs relative free energy ΔG (kcal/mol), Boltzman weighting factor p (%) of low energy tautomers of **1** calculated in the B3LYP/6-311**G level

	Gas		Chloroform		Dimethylsulfoxide	
Tautomer	ΔG	p	ΔG	p	ΔG	p
A	0	90	0	87	0	90
B	1.35	10	1.12	13	1.32	10

3.2. Frontier orbitals and descriptors

The HOMO and LUMO molecular orbitals for the *A* and *B* tautomers are located on the pyran ring (Fig. 3). Conjugation provides a flat structure for this ring. It is interesting to see how the charge distribution changes during tautomeric transformations. In the tautomeric transformation from form *A* to *B*, the negative charge on the O3 atom increases, and that on the O4 atom decreases (Supplementary Information S3). In the *B* form, the charges on the atoms C5, C6, and C7 increase, and on the C27, H44 atoms decrease. It follows from these data that the chemical properties change during the tautomeric transition.

The pyrone **1** molecule contains several functional groups. Their reactions can be described using descriptors. Form *B* was found to have higher ionization energy, electron affinity, chemical potential, electrophilic index, and energy band gap than Form *A* (Table 2). The dipole moment is higher for form *A*, and the softness of both molecules is the same.

Table 2
Calculated ionization energy (*I*), electron affinity (*A*), energy band gap (|GAP|), chemical potential (μ), global softness (*S*), global electrophilicity index (ω), and dipole moment (*M*) for tautomeric forms *A* and *B* of compound **1.**

Tautomer	*I*, eV	*A*, eV	|GAP|	μ, eV	*S*, eV	ω, eV	M, D
A	8.661	0.803	4.618	-4.732	0.127	2.850	3.414
B	8.795	0.883	4.693	-4.839	0.126	2.960	1.935

The calculation of the local electrophilic indices makes it possible to estimate the reactivity of the atoms for two tautomeric forms (Supplementary Information S3). The electrophilic index of oxygen atoms is higher for the *A* form. For the carbon atoms C5, C6, C7, and C27, the electrophilicity index is higher for form *A*. It should be emphasized that the C6 atom is highly reactive. Detailed analysis of chemical descriptors allows finding new ways to obtain drugs with desired properties.

3.3. NBO Analysis

The molecular orbitals are similar for the two tautomeric forms, but there is an orbital $\sigma(2)_{C6–C7}$ = $0.8137(sp^{1.00}d^{0.00})_{C6} + 0.5812(sp^{1.00}d^{0.00})_{C7}$ in form *A*, which is not in form *B*. In form *B* there is an orbital $\sigma(2)_{O3–C7}$ = $0.8605(sp^{1.00}d^{0.00})_{O3} + 0.5095(sp^{1.00}d^{0.00})_{C7}$, which is not in form *A*. These extra orbitals are of π character and indicate an increase in bond order.

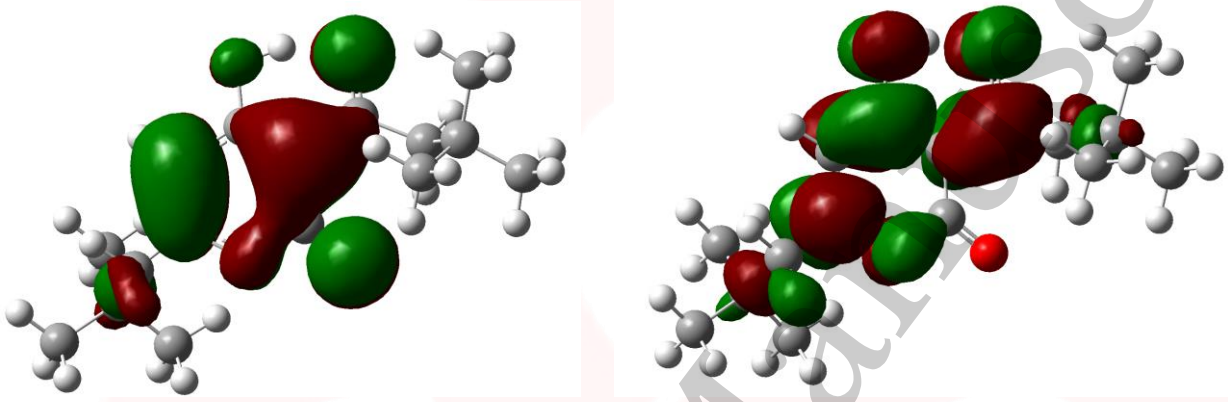

HOMO LUMO

1

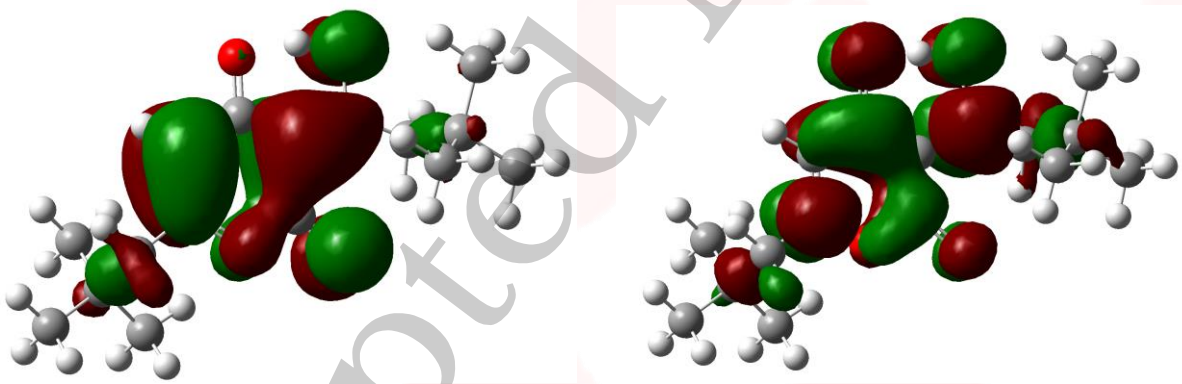

HOMO LUMO

2

Fig. 3. Molecular orbital surfaces for tautomeric forms *A* (1) and *B* (2) of compound **1**.

In form *A*, significant interactions of C6–C7, C8–C10 bond orbitals with antibonding orbitals of the O2–C5, O4–C27, C6–C7 σ_2(C6–C7)→σ^*_2(O2–C5), σ_2(C6–C7)→σ^*_2(O4–C27), σ_2(C8–C10)→σ^*_2(C6–C7) with stabilization energies 34.18, 31.20, and 24.96 kcal/mol (Supplementary Information S4). Additionally, the molecule has lone electron pairs of oxygen atoms interactions with O2–C5, C5–C6, C6–C7, and O3–H44 bonds,

n(LP_2O1)→σ_1*(O2–C5), n(LP_2O2)→σ_1*(O1–C5), n(LP_2O2)→σ_2*(C5–C6), and n(LP_2O4)→σ_1*(O3–H44) with energies 29.25, 40.10, 15.56, and 42.96 kcal/mol.

In the tautomeric form *B*, the delocalization of electrons is maximal for the C8–C10 bond and is distributed over the antibonding orbitals O3–C7 σ_2(C8–C10)→σ^*_2(O3–C7) with the stabilization energies 27.83 kcal/mol. Additionally, the molecule has lone electron pairs of oxygen atom interactions n(LP_2O1)→σ_2*(O2–C5), n(LP_2O1)→σ_1*(C8–C10), n(LP_2O2)→σ_1*(O1–C5), n(LP_2O2)→σ_1*(C5–C6), and n(LP_2O3)→σ_1*(O4–H44) with energies 31.36, 34.08, 37.96, 15.85, and 63.18 kcal/mol.

3.4. Vibrational analysis

The determination of the type of vibration in the experimental spectra was carried out by analyzing the potential energy, the atomic displacements, and the comparison with related compounds [29, 30]. The experimental and calculated vibrational spectra for two tautomers *A* and *B* of compound **1** are shown in Figs. 4 and 5 and Table 3.

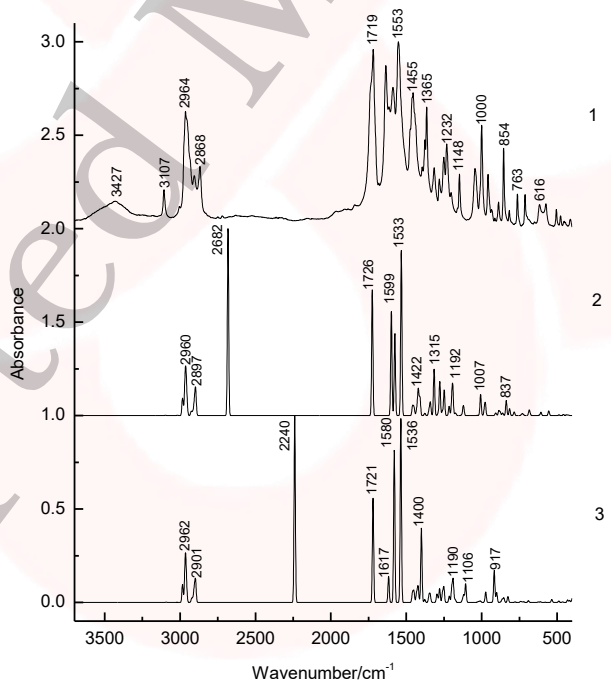

Fig. 4. Experimental IR spectra of crystalline compound **1** (1) and calculated IR spectra of tautomeric forms *A* (2) and *B* (3). The theoretical spectra were modeled using Lorentz functions centered on the calculated frequencies, scaled by a factor of 0.96 and an FWHM of 10 cm^{-1}.

The sharp medium-intensity peak in the IR spectrum at 3107 cm^{-1} and the frequency of 3108 cm^{-1} in the Raman spectrum refer to *CH* stretching vibrations (C8−H9 bond). Experimental frequencies in the region 3100−2960 cm^{-1} in vibrational spectra refer to $\nu_{as}(CH_2)$ and $\nu_{as}(CH_3)$ stretching vibrations. The symmetrical stretching vibrations of the methyl and methylene groups cause frequencies in the range of 2910−2860 cm^{-1} in the experimental spectra.

Stretching of carbonyl groups without H-bonds (C5=O bond) causes a band at 1719 cm^{-1} in the experimental IR and Raman spectra (Figs. 4 and 5). The stretching vibrations of the carbonyl group forming the H-bond (C3=O7 bond) are shifted to the low-frequency region of 1636 cm^{-1}.

The bands in the region 1460−1400 cm^{-1} in the experimental spectra are due to the $\delta_{as}(CH_3)$ and $\delta_{as}(CH_2)$ bending vibrations. Symmetrical bending vibrations $\delta_s(CH_3)$ and $\delta_s(CH_2)$ cause bands in the region 1400−1340 cm^{-1}. The frequency at 1315 cm^{-1} in the experimental IR spectrum and the band at 1318 cm^{-1} in the experimental Raman spectrum are due to the wagging vibrations of the methylene groups.

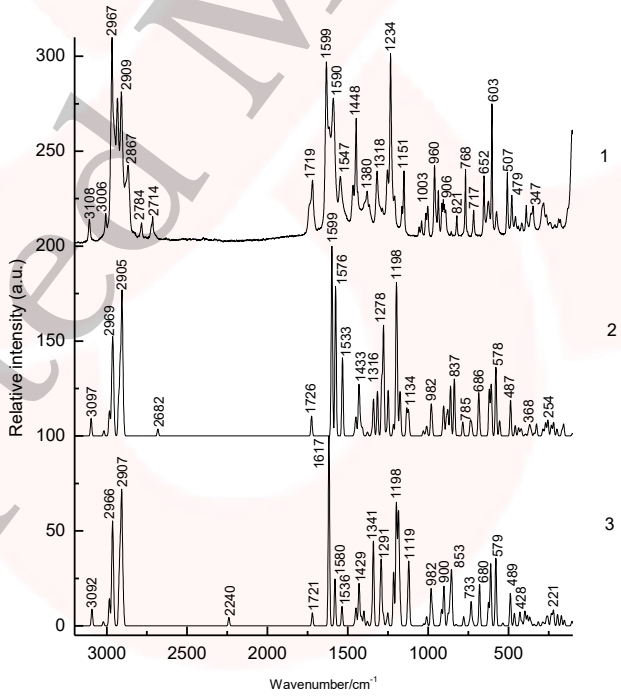

Fig. 5. Experimental Raman spectra of crystalline compound **1** (1) and theoretical Raman spectra of tautomeric forms *A* (2) and *B* (3). The theoretical spectra were modeled using Lorentz functions centered on the calculated frequencies, scaled by a factor of 0.96 and an FWHM of 10 cm^{-1}.

Stretching vibrations of the *CO* and *CC* bonds of the pyran ring (C5−O1 and C5−C6 bonds) cause frequencies between 1290 and 1150 cm^{-1} in the experimental spectra. The bands in the region of 1060 to 1000 cm^{-1} in the experimental spectra were attributed to the deformation of the *CCH* angles and stretching of the *CC* bonds.

The rocking vibrations of the methyl groups $\rho(CH_3)$ cause bands between 960 and 880 cm^{-1} in the experimental IR and Raman spectra. Bands of average intensity in the region of 860−760 cm^{-1} in the experimental spectra refer to *CO* and *CC* bonds (C5−O1 and C5−C6 bonds) stretching vibrations.

Table 3
Observed and calculated wavenumders $\nu(cm^{-1})$, the intensity of the bands in the IR spectra I (km/mol) and relative intensity of the bands in the Raman spectra J (a.u.) and assignments for the tautomeric forms *A* and *B* of compound **1** in the gas phase by using the B3LYP/6−311++G** method.

Experimental		B3LYP/6−311++G** method						
IR	Raman	*A*			*B*			Assignments
ν	ν	ν	I	J	ν	I	J	
3427w								
3107w	3108w	3097	1.1	9.2	3092	1.1	8.8	νC8−H9
3004vw	3006w	3018	1.0	2.7	3021	0.6	2.2	νC28−H29 ν_{as} CH_2
		2985	30.6	5.7	2984	26.8	5.5	νC19−H20 ν_{as} CH_3
		2984	26.3	4.7	2984	33.3	4.8	νC32−H33 ν_{as} CH_3
		2980	17.6	4.8	2983	16.2	4.2	νC40−H41 ν_{as} CH_3
		2969	64.4	14.8	2969	55.8	10.8	νC23−H24 ν_{as} CH_3
		2966	33.2	11.1	2966	43.1	13.4	νC15−H16 ν_{as} CH_3
2964s	2967s	2964	43.8	12.8	2965	30.9	7.2	νC11−H12 ν_{as} CH_2
		2963	26.0	6.0	2963	45.5	12.3	νC36−H37 ν_{as} CH_3
		2961	3.1	2.1	2962	70.0	18.6	νC19−H21 ν_{as} CH_3
		2960	79.0	21.3	2961	1.9	1.8	νC32−H34 ν_{as} CH_3
2956sh		2957	8.0	1.8	2957	6.7	1.8	νC23−H25 ν_{as} CH_3
		2956	3.8	1.5	2956	4.4	1.2	νC15−H17 ν_{as} CH_3
		2954	4.7	1.9	2956	22.0	2.7	νC32−H34 ν_{as} CH_3
		2953	26.1	2.9	2955	3.2	1.2	νC40−H42 ν_{as} CH_3
	2933m	2926	15.8	18.8	2923	14.8	20.7	νC28−H29 ν_{as} CH_2
		2916	14.1	37.1	2916	14.2	35.8	νC11−H12 ν_{as} CH_2
	2909m	2908	19.5	22.9	2908	20.3	21.8	νC19−H21 ν_{s} CH_3
2906m		2905	26.0	50.4	2907	23.9	42.3	νC32−H33 ν_{s} CH_3
		2900	25.1	12.2	2901	26.5	1.4	νC23−H24 ν_{s} CH_3

		2899	28.5	1.0	2900	26.0	9.6	νC40−H41 ν_s CH_3
		2897	28.9	2.2	2896	28.7	3.4	νC15−H16 ν_s CH_3
2868m	2867w	2895	31.1	4.6	2896	29.3	4.5	νC36−H37 ν_s CH_3
2675vw	2784vw	2682	709.1	3.7	2240	787.7	4.4	νO3−H44
2666vw	2714vw							
2666vw								
2631vw								
2608vw								
2568vw								
2524vw								
2372vw								
2364vw								
2355vw								
2338vw								
1737sh	1738sh							
1719vs	1719m	1726	479.7	10.4	1721	440.3	6.8	νC5=O2
1683w								
1636s	1633vs	1599	394.4	100.0	1617	110.3	100.0	νC3=O7
1615w	1617sh							
1588m	1590m	1576	311.0	78.6	1580	641.7	24.6	βO3−H44
1553vs	1547m	1533	626.8	41.2	1536	775.5	10.3	νC6−C7
1474sh								
1462sh	1467m	1460	18.0	0.7	1460	21.1	0.4	βC32−H33 δ_{as} CH_3
1455m		1458	17.0	0.9	1458	19.6	0.6	βC19−H20 δ_{as} CH_3
		1452	12.7	1.5	1451	19.4	1.6	βC36−H39 δ_{as} CH_3
		1451	4.9	5.1	1450	14.0	3.7	βC15−H16 δ_{as} CH_3
		1449	6.7	1.5	1449	6.6	1.4	βC11−H12 δ_{as} CH_2
1445sh	1448m	1447	11.3	2.6	1447	10.0	3.4	βC28−H29 δ_{as} CH_2
1437sh	1438sh	1433	7.8	11.7	1432	20.9	5.3	βC40−H41 δ_{as} CH_3
		1430	8.7	6.0	1432	15.3	6.1	βC32−H33 δ_{as} CH_3
		1429	3.4	7.4	1429	2.0	7.5	βC15−H16 δ_{as} CH_3
		1428	6.4	4.2	1428	3.5	5.0	βC19−H20 δ_{as} CH_3
		1425	0.4	0.2	1425	0.4	0.2	βC23−H25 δ_{as} CH_3
		1424	2.4	0.3	1424	2.0	0.0	βC36−H37 δ_{as} CH_3
		1422	77.7	4.5	1422	63.1	1.3	βC28−H29 δ_s CH_2
		1417	32.8	2.2	1415	6.4	4.6	βC11−H12 δ_s CH_2
1394vw		1409	64.0	4.0	1400	312.5	7.8	βC28−H29 δ_s CH_2
1376w	1380m	1379	4.3	1.4	1379	5.8	1.1	βC19−H21 δ_s CH_3
1365m	1369sh	1376	4.7	0.8	1377	6.8	1.3	βC32−H35 δ_s CH_3
	1365sh	1351	7.6	1.7	1351	6.2	3.7	βC19−H20 δ_s CH_3
		1349	6.0	0.3	1350	14.3	0.3	βC32−H33 δ_s CH_3
		1347	7.3	0.3	1346	8.3	1.2	βC23−H24 δ_s CH_3
		1344	7.5	0.6	1345	8.6	0.6	βC36−H37 δ_s CH_3
		1340	44.1	18.9	1341	23.0	43.3	νC5−O1
1315w	1318m	1316	176.4	23.6	1298	30.1	13.8	βC28−H29 wag CH_2
		1289	8.9	29.5	1291	13.8	29.5	βC11−H12 wag CH_2
1282w	1285vw	1278	129.0	57.2	1279	58.2	5.9	νC6−C7

		1261	16.8	2.1	1260	39.7	1.7	βC28−H29 wag CH_2
1251w	1253m	1249	97.4	23.9	1251	63.1	6.6	νC6−C27
1232m	1234vs	1216	34.5	6.1	1215	26.9	28.2	νC6−C27
1203w	1208w	1198	57.3	72.3	1198	60.9	61.8	βC23−H24 wag CH_3
		1192	98.5	21.7	1190	90.7	22.0	βC32−H35 wag CH_3
		1177	4.7	10.8	1184	8.2	49.9	νC5−C6
		1174	2.9	12.4	1176	7.5	3.0	βC23−H24 τw CH_3
1161sh	1163w	1170	4.2	3.2	1174	3.4	9.7	νC5−O1
1148m	1151m	1134	2.0	14.2	1128	11.0	8.1	βC8−H9
		1123	25.1	11.1	1122	3.4	16.2	βC28−H29 τw CH_2
	1056vw	1119	19.1	3.6	1119	29.0	18.1	βC11−H12 τw CH_2
1044m	1041w	1030	0.7	2.7	1106	78.5	0.4	βC40−H41
	1014w	1017	0.6	0.8	1027	2.2	1.0	βC23−H24
		1011	1.2	1.7	1018	4.0	0.3	βC36−H39
		1009	15.2	2.4	1010	1.7	2.7	βC23−H24 τw CH_3
1000m	1003w	1007	64.9	1.3	1008	4.1	2.3	δO3−H44
		982	22.5	13.9	982	1.2	18.8	νC7−C8
959m	960m	976	41.1	7.2	973	44.3	7.2	νO1−C10
935w	937w	928	0.1	0.1	928	0.5	0.1	γC32−H33 ρ CH_3
929sh		926	0.0	0.1	926	0.2	0.1	γC23−H24 ρ CH_3
912vw	914w	910	3.7	2.7	917	135.1	8.4	γC28−H29 ρ CH_3
	906w	907	4.9	2.2	907	1.4	1.3	γC19−H20 ρ CH_3
		903	2.1	8.9	903	2.9	7.7	νC14−C23
	899w	902	0.4	4.4	902	3.7	3.1	νC31−C36
888w	891w	887	17.5	9.3	900	35.3	10.5	νC5−C6, νC5−O1
		877	13.4	12.9	876	1.0	6.3	νC14−C19
	861sh	862	3.2	3.9	865	12.8	11.0	νC14−C15
854m	856vw	861	6.9	22.6	857	5.1	14.3	νC10−C11
	844sh	837	57.4	30.0	853	16.6	18.5	νO1−C5
817w	821w	815	26.3	0.3	826	25.0	0.7	γC8−H9
779sh	768m	785	13.7	7.4	779	2.5	4.8	ρC27−O4
763w	754sh	738	2.6	7.6	742	4.5	2.4	νC8−C10
		729	7.2	5.7	733	2.1	12.5	ρC7−O3
713w	717w	720	1.4	0.2	721	2.8	1.9	νC10−C11
697sh		686	18.3	21.3	691	7.4	0.6	νC27−C28
686sh	652m	680	6.8	3.9	680	0.3	21.8	ρC7−O3
650sh	625w	620	1.1	24.4	625	2.2	12.2	νC10−O1
616w	603m	607	12.3	27.0	611	2.8	32.7	ρC7−O3
574w	575w	578	0.4	36.4	579	0.8	35.6	νC10−C11
544sh		555	17.8	8.0	535	12.8	1.5	β_R
536sh								
529sh								
505w	507m							
477vw	479w	487	2.6	18.8	489	6.0	17.1	β_R
453vw	456w	458	4.1	5.4	464	2.0	6.6	β_R
445vw		438	3.1	4.3	430	10.3	2.6	β_R
436vs	439vw	426	1.7	1.9	428	0.0	4.8	β_R

412vw	418vw	419	0.2	3.1	417	8.3	2.4	τ_R
		396	0.1	0.7	400	14.6	5.2	τ_R
	389w	391	3.1	0.5	395	4.8	3.9	βC27−O4
	381sh	375	3.5	2.4	383	11.1	5.5	ρC5=O2
		368	0.3	5.3	369	0.4	4.4	βC14−C19
	359sh	359	0.6	2.9	360	3.0	1.8	βC27−C28
	347w	340	2.1	1.6	340	0.9	0.8	γC10−C11
		326	6.6	6.4	315	3.0	2.1	βC27−O4
	288sh	287	0.4	3.0	288	0.2	1.7	τC14−C15
	281w	283	1.5	0.6	283	0.2	0.3	τC31−C32
		280	0.3	0.4	280	0.2	0.2	τC14−C15
		276	0.1	1.1	277	0.1	0.9	τC14−C23
	264vw	269	2.2	6.5	265	2.1	2.8	τ_R
		258	1.0	2.6	260	0.3	2.2	τC14−C23
		254	0.9	6.5	255	0.5	3.5	β_R
	241vw	235	1.3	4.5	236	0.4	4.3	τC14−C23
		230	0.2	1.9	230	1.5	3.7	τC31−C40
		220	0.6	6.0	221	0.3	6.1	τC14−C15
	211vw	219	0.3	1.1	219	0.6	2.0	τ_R
	188vw	199	3.6	3.6	195	0.7	5.9	τ_R
	178vw	167	0.3	3.1	171	1.0	5.4	τ_R
	168vw	157	2.7	6.2	152	2.5	3.0	τ_R
	105vw	103	0.2	1.3	105	0.9	2.4	τ_R

Abbreviations: vs, very strong; s, strong; m, medium; w, weak; vw, very weak; ν, stretching; β, deformation in plane; γ, deformation out of plane; wag, wagging; τ, torsion; β_R, deformation ring; τ_R, torsion ring; ρ, rocking; τw, twisting; δ, deformation; a, antisymmetric; s, symmetric.

The band at 713 cm^{-1} in the experimental spectra refers to the stretching vibrations of the CC bonds (C10−C11 bond). Bending vibrations of the pyran ring cause bands in the 620−470 cm^{-1} region in the experimental spectra. Bending and torsional vibrations of the pyran ring cause bands in the 500−100 cm^{-1} region of IR and Raman spectra.

It is important to know what changes occur in the vibrational spectra of compound **1** during the tautomeric transformation. The spectra of tautomeric forms *A* and *B* are similar (Figs. 4 and 5). For tautomers *A* and *B*, the frequencies of most bands remain unchanged, but their intensity changes. Bands 1726, 1599, 1576, 1533, 1422, 1315, and 1192 cm^{-1} of the form *A* IR spectrum are shifted to frequencies 1721, 1617, 1580, 1536, 1400, 1341, and 1190 cm^{-1} of the form *B* IR spectrum (Fig. 4). Bands 1726, 1599, 1576, 1533, 1433, 1340, 1316, 1278, 1249, 1198, 837, 686, 607, 578, 487 cm^{-1} in the Raman spectrum of form *A* are shifted to frequencies 1721, 1617, 1580, 1536, 1429, 1341, 1291, 1198, 853, 680, 579, 489 cm^{-1} in the Raman spectrum of form *B* (Fig. 5).

The theoretical spectra agree with the experimental vibrational spectra of tautomer *A* in a wide frequency range (Figs. 4 and 5). Thus, the use of the DFT approximation for the considered molecular system is correct.

4. Hydrogen bond

Compound **1** has a strong H-bond with a cyclic chelate structure. The enol form of β-diketones is a well-known case of a 6-membered ring (chelate) with a strong resonance-assisted H-bond [31−35]. The characteristic spectral features observed for such structures are that instead of pronounced carbonyl stretching bands, strong absorption bands are present in the region of 1580-1630 cm^{-1} [16]. The stretching of the OH bond band shifts up to 2200 cm^{-1} [16].

Additionally, due to the resonance of two enol tautomers (both are chelate enol forms), this structural fragment can be considered a quasisymmetric O···H···O hydrogen bond. This bond has a broad and shallow potential well with two minima, which leads to a series of diffuse absorption bands scattered over a wide wavenumber region.

The analysis of the observed IR spectrum **1** in the region of 2700−2000 cm^{-1} shows that there are several weak bands, *ν(OH)* (Fig. 6). The calculated *ν(OH)* frequencies after scaling are 2682 and 2240 cm^{-1} for tautomers *A* and *B*, respectively, and they are in the range between 2700 and 2200 cm^{-1}. An empirical formula is proposed that establishes a correlation between the frequencies *ν(OH)* observed and those calculated in the harmonic approximation: $\nu_{obs} = -757 + 1.173\ \nu_{harm}$ [35]. The calculation by this formula yields *ν(OH)* frequencies of 2520 and 1980 cm^{-1} for tautomers *A* and *B*, respectively. In the experimental IR spectrum of compound **1**, the band 2524 cm^{-1} is observed, which can be attributed to *ν(OH)* vibrations. The shift of this band to low frequencies depends on the strength of the intramolecular H-bond. We see that in the most energy-stable tautomer *A*, the H-bond is weaker.

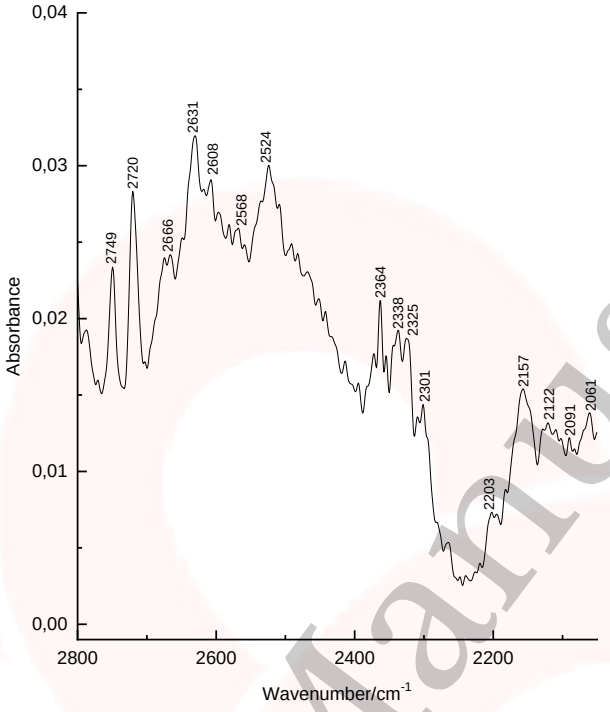

Fig. 6. The experimental IR spectrum of compound **1** in the region 3600−2700 cm^{-1}.

This conclusion is consistent with the fact that the H-bond length for *A* and *B* tautomers is 2.473 and 2.418 Å, respectively. The strength of the H-bond can be described using Wiberg bond indices 0.158 (tautomer *A*) and 0.204 (tautomer *B*) [26]. These values of the Wiberg indices indicate that strong H-bonds are formed in compound **1** for both tautomers. It appears from our data that there is a correlation between the frequencies *ν(OH)* calculated in the harmonic approximation and the Wiberg indices. The stronger the H-bond, the lower the ν(OH) frequency and the higher the Wiberg index.

The strength of the intramolecular H-bond in compound **1** can be estimated as the interaction $n(LP_2O4)\rightarrow\sigma_1^*(O3–H44)$ with the energy 42.96 kcal/mol of the tautomer *A* and $n(LP_2O3)\rightarrow\sigma_1^*(O4–H44)$ with energy 63.18 kcal/mol of tautomer *B*. The energy of the donor-acceptor interaction of the H-bond is larger for the *B* tautomer; therefore, it is stronger. Interactions $\sigma_1(O3–H44)\rightarrow\sigma^*_1(C7–C8)$, $\sigma_2(C6–C7)\rightarrow\sigma^*_2(O4–C27)$, $\sigma_2(C6–C7)\rightarrow\sigma^*_2(C8–C10)$, $\sigma_2(C8–C10)\rightarrow\sigma^*_2(C6–C7)$ with energies 5.83, 31.20, 7.49, 24.96 kcal/mol (tautomer *A*), and $\sigma_2(C8–C10)\rightarrow\sigma^*_2(O3–C7)$ with energy 27.83 kcal/mol (tautomer *B*) are realized due to the conjugation of bonds in a six-membered ring.

5. Conclusions

In conclusion, the correlation between the structure and H-bonding was established in 3-(3,3-Dimethylbutanoyl)-4-hydroxy-6-neopentyl-2H-pyran-2-one. For pyrone **1**, the X-ray diffraction, DFT-calculations and IR, Raman spectroscopy revealed the most favourable tautomeric form *A*. The content of tautomer *B* increases in the nonpolar solvent but does not exceed 13%.

As can be seen from our calculations and experimental X-ray data, the pyran ring of the molecule is flat. A satisfactory agreement is observed between the calculated geometrical parameters of tautomer *A* and the experimental X-ray data.

The calculation of the normal vibrations by the DFT method gives a detailed description of the dynamics of pyrone **1**. The intensities of the bands in the IR spectra show high sensitivity to the H-bond in compound **1**.

The HOMO and LUMO orbitals of the acid molecule are located on the pyran ring. During tautomeric transformations, there is a significant delocalization of the charge, which modifies the reactivity of the molecule.

The reactivity of compound **1** was characterized using descriptors. Form *B* was found to have higher ionization energy, electron affinity, chemical potential, and electrophilic index than Form *A*. The dipole moment is higher for Form *A*, and the softness of the two molecules is the same.

The obtained results allow us to better understand the interplay between the tautomeric flexibility of the pyrone ring and its H-bonding, providing a new approach for rational design of drugs with desired properties.

Acknowledgement

The work was carried out within the framework of the state assignment " Petrochemistry and Catalysis. Rational use of carbon-containing raw materials ", No. 121031300092-6.

References

[1] Penta, S. Dehydroacetic Acid and Its Derivatives: useful synthons in organic synthesis. 1st ed. Elsevier Ltd, **2017**.

[2] Dobler, D.; Leitner, M.; Moor, N.; Reiser, O. 2-Pyrone – a privileged heterocycle and widespread motif in nature. Eur. J. Org. Chem. **2021**, 61801−6205. [doi: 10.1002/ejoc.202101112].

[3] Tian, R.D.; Sheng, M.K.; Zhao, Y.F.; Wen, C.N.; Liu, M.; Ma, J. α-Pyrone derivatives from the endophytic fusarium sp. L33 isolated from dioscorea opposita. Phytochem. Lett. **2024**, *62*, 14−17. [doi: 10.1016/j.phytol.2024.06.002]

[4] Colin, M.J.; Aguilar, M.A.; Martin, M.E. A theoretical study of solvent effects on the structure and UV-vis spectroscopy of 3-hydroxyflavone (3-HF) and some simplified molecular models. ACS Omega. **2023**, *8*, 19939−19949. [doi: 10.1021/acsomega.3c01906]

[5] Fujihara, K.; Hashimoto, T.; Sasaki, H.; Koyama, K.; Kinoshita, K. Inhibition of Aβ aggregation by naphto-γ-pyrone derivatives from a marine-derived fungus, aspergillus sp. MPUC239. J. Nat. Med. **2023**, *77*, 516−522. [doi: 10.1007/s11418-023-01696-9]

[6] Kawsar, S.M.A.; Hosen, M.A.; Chowdhury, T.S.; Rana, K.M.; Fujii, Y.; Ozeki, Y.. Thermochemical, PASS, molecular docking, drug-likeness and in silico admet prediction of cytidine derivatives against HIV-1 reverse transcriyase. Rev. Chim. Lett., **2023**, *72*, 159−178. [doi: 10.37358/Rev.Chim.1949]

[7] Tabassum, R.; Kawsar, S.M.A.; Alam, A.; Saha, S.; Hosen, A.; Hasan, I.; Prinsa; Mohhamed, C. Synthesis, spectral characterization, biological, FMO, MEP, molecular docking, and molecular dynamic simulation studies of cytidine derivatives as antimicrobial and anticancer agents. Chem. Phys. Impact. **2024**, *9*, 100724. [doi: 10.1016/j.chphi.2024.100724]

[8] Akter N.; Bourougaa, L.; Oussaf, M.; Bhowmic, R.C.; Uddin, K.M.; Bhat, A.R.; Ahmed, S.; Kawsar, S.M.A. Molecular docking, ADME-Tox, DFT and molecular dynamic simulation of butyroyl glucopyranoside derivatives against DNA gyrase inhibitors as antimicrobial agents. J. Mol. Struct., **2024**, *1307*, 137930. [doi: 10.1016/j.molstruc.2024.13730]

[9] Guo, Z.; Chen, B.; Chen, D.; Deng, X.; Yuan, J.; Zhang, S.; Xiong, Z.; Xu, J. New isocoumarin and pyrone derivatives from the Chinese Mangrove plant rhizophora mangle-associated fungus phomopsis sp. DHS-11. Molecules. **2023**, *28*, 3756. [doi: 10.3390/molecules28093756]

[11] Jiang, W.; Hou, W.; Yan, C.; Nie, Z.; Chang, Q.; Li, X.; Liu, W. Synthesis and performance of deep-red phosphorescent iridium complexes with pyrone as an auxiliary ligand. Molecules. **2024**, *29*, 3183. [doi: 10.3390/molecules29133183]

[12] Kohanov, Z.A.; Shuvo, S.I.; Lowell, A.N. Reioselective annulations of 6-carboxy-substituted pyrones asa two-carbon unit in formal [4 + 2]cycloaddition reactions. J. Org. Chem. **2024**, *89*, 9557−9568. [doi: 10.1021/acs.joc.4c01044]

[13] Chalaca, M.Z.; Figuerola-Villar, J.D. A theoretical and NMR study of the tautomerism of dehydroacetic acid. J. Mol. Struc., **2000**, *554*, 225−231. [doi: 10.1016/S0022-2860(00)00674-8.]

[14] Gorodetsky, M.; Luz, Z.; Mazur, Y. Oxygen-17 nuclear magnetic resonance studies of the equilibria between the enol forms of β-diketones. J. Am. Chem. Soc. **1967**, *89*, 1183−1189. [doi: 10.1021/ja00981a026].

[15] Billes, F.; Eleckova, L.; Mikosch, H.; Andruch, V. Vibrational spectroscopic study of dehydroacetic acid and its cinnamoyl pyrone derivatives. Spectrochim. Acta Part A. **2015**, *146*, 97−112. [doi: 10.1016/j.saa.2015.03.010.]

[16] Emsley, J. The composition, structure and hydrogen bonding of the β-diketones. Complex Chemistry. **1984**, *57*, 147−191. [doi: 10.1007/BFb0111456.]

[17] Yamada, K. Infrared and ultraviolet spectra of α- and γ-pyrones. Bull. Chem. Soc. Japan. **1962**, *35*, 1323−1329. [doi: 10.1246/bcsj.35.1323.]

[18] Tykhanov, D.A.; Serikova, I.I.; Yaremenko, F.G.; Roshal, A.D. Structure and spectral properties of cinnamoyl pyrones and theirs vinylogs. Cent. Eur. J. Chem. **2010**, *8*, 347−355. [doi: 10.2478/s11532-009-0138-4.]

[19] Nomerotskaya, E.I. (**2020**). Polyfunctional alpha-pyrones: direct synthesis from carboxylic acids and properties. [Unpublished master's thesis, Moscow State University].

[20] Sun, X.; Gong, M.; Huang, M.; Li, Y.; Kim, J.K.; Kovalev, V.V.; Shokova, E.A.; Wu, Y. One-pot synthesis of pyrones from aromatic ketones/heteroarenes and carboxylic acids. J. Org. Chem. **2020**, *85*, 15051−15061. [doi: 10.1021/acs.joc.0c01924.]

[21] https://plastics-polymer-analysis.com/ru/

[22] Becke, A.D. Density-functional thermochemistry. III. The role of exact exchange. J. Chem. Phys. **1993**, *98*, 5648−5652. [doi: 10.1063/1.464913.]

[23] Lee, C.; Yang, W.; Parr, R.G. Development of the Colle-Salvetti correlation-energy formula into a functional of the electron density. Phys. Rev. B **1988**, *37*, 785−789. [doi: 10.1103/PhysRevB.37.785.]

[24] Frisch, M.J.; Trucks, G.W.; Schlegel, H.B.; Scuseria, G.E.; Robb, M.A.; Cheeseman, J.R.; Scalmani, G.; Barone, V.; Mennucci, B.; Petersson, G.A.; Nakatsuji, H.; Caricato, M.; Li, X.; Hratchian, H.P.; Izmaylov, A.F.; Bloino, J.; Zheng, ; Sonnenberg, J.L.; Hada, M.; Ehara, M.; Toyota, K.; Fukuda, R.; Hasegawa, J.; Ishida, M.; Nakajima, T.; Honda, Y.; Kitao, O.; Nakai, H.; Vreven, T.; Montgomery, J.A.; Peralta, J.E.; Ogliaro, F.; Bearpark, M.; Heyd, J.J.; Brothers, E.; Kudin, K.N.; Staroverov, V.N.; Keith, T.; Kobayashi, R.; Normand, J.; Raghavachari, K.; Rendell, A.; Burant, J.C.; Iyengar, S.S.; Tomasi, J.; Cossi, M.; Rega, N.; Millam, J.M.; Klene, M.; Knox, J.E.; Cross, J.B.; Bakken, V.; Adamo, C.; Jaramillo, J.; Gomperts, R.; Stratmann, R.E.; Yazyev, O.; Austin, A.J.; Cammi, R.; Pomelli, C.; Ochterski, J.W.; Martin, R.L.; Morokuma, K.; Zakrzewski, V.G.; Voth, G.A.; Salvador, P.; Dannenberg, J.J.; Dapprich, S.; Daniels, A.D.; Farkas, O.; Foresman, J.B.; Ortiz, J.V.; Cioslowski, J.; Fox, D.J.Gaussian 09 Revision C.01, Gaussian Inc., Wallingford CT. **2010**.

[25] Jamroz, M.H. Vibrational energy distribution analysis (VEDA): scopes and limitations. Spectrochim. Acta. **2013**, *114*, 220−230. [doi: 10.1016/j.saa.2013.05.096.]

[26] Glendening, E.D.; Landis, C.R.; Weinhold, F. Natural bond orbital methods. Comput. Mol. Sci. 2. **2012**. 1−42.

[27] Yang, W.; Parr, R.G. Hardness, softness, and the fukui function in the electronic theory of metals and catalysis. PNAS. **1985**, *82*, 6723−6726. [doi: 10.1073/pnas.82.20.6723.]

[28] Tomasi, J., Perisco, M. Molecular interactions in solution: an overview of methods based on continuous distributions of the solvent. Chem. Rev. **1994**, *94*, 2027−2094. [doi: 10.1021/cr00031a013.]

[29] Castillo, M.V.; Rudyk, R.A.; Davies, L., Brandan, S.A. Analysis of the structure and the FT-IR and Raman spectra of 2-(4-nitrophenyl)-4H-3,1-benzoaxin-4-one. Comparison with the chlorinated and methylated derivatives. J. Mol. Struct., **2017**, *1140*, 2−11. [doi: 10.1016/j.molstruc.2016.08.070.]

[30] Chahar, F.C.; Alvarez, P.A.; Zampini, C.; Isla, M.I.; Brandan, S.A. Experimental and DFT studies on 2',4'-dihydroxychalcone, a product isolated from *Zuccagnia punctata Cav.* (Fabaceae) medicinal plant. J. Mol. Struct. **2020**, *1201*, 127221. [doi: 10.1016/j.molstruc.2019.127221.]

[31] Gilli, G.; Bellucci, F.; Ferretti, V.; Bertolasi, V. Evidence for resonance-assisted hydrogen bonding from crystal-structure correlations on the enol form of the β-diketone fragment. J. Am. Chem. Soc. **1989**, *111*, 1023−1028. [doi: 10.1021/ja00185a035.]

[32] Rusinska-Roszak, D. Intramolecular O-H···C=O hydrogen bond energy via the molecular tailoring approach to RAHB structures. J. Phys. Chem. A. **2015**, *119*, 3674−3687. [doi: 10.1021/acs.jpca.5b02343.]

[33] Guevara-Vela, J.M.; Romero-Montalvo, E.; Costales, A.; Pendas, A.M.; Rocha-Rinza, T. The nature of resonance-assisted hydrogen bonds: a quantum chemical topology perspective. Phys. Chem. Chem. Phys. **2016**, *18*, 26383−26390. [doi: 10.1039/C6CP04386K.]

[34] Hansen, P.E.; Spanget-Larsen, J. NMR and IR Investigations of strong intramolecular hydrogen bonds. Molecules. **2017**, *22*, 552. [doi: 10.3390/molecules22040552.]

[35] Wiberg, K.A. Application of the pople-santry-segal CNDO method to the cyclopropylcarbinyl and cyclobutyl cation and to bicyclobutane. Tetrahedron. **1968**, *24*, 1083−1096. [doi: 10.1016/0040-4020(68)88057-3.]